Magnetization density in URhAl-evidence for hybridization effects

1992 J. Phys.: Condens. Matter 4 829

(http://iopscience.iop.org/0953-8984/4/3/022)

J. Phys.: Condens. Matter 4 (1992) 829–846. Printed in the UK

Magnetization density in URhAl—evidence for hybridization effects

J A Paixão*†, G H Lander†, P J Brown‡, H Nakotte§, F R de Boer§ and E Brück§

† Commission of the European Communities, Institute for Transuranium Elements, Karlsruhe, Postfach 2340, D-7500, Federal Republic of Germany

‡ Institut Laue–Langevin, 156X, 38042 Grenoble, France

§ Van der Waals–Zeeman Laboratorium, University of Amsterdam, Valckenierstraat 65, 1018 XE Amsterdam, The Netherlands

Received 27 June 1991

Abstract. URhAl is one of a large class of uranium compounds with the hexagonal ZrNiAl structure. It becomes ferromagnetic at 27 K and the ordered moment is found to be 0.94 μ_B per formula unit. We have performed experiments with polarized neutrons in order to measure the magnetization density in the unit cell. A crystallographic study gives atomic positions in agreement with previous work, but we find that the crystals, which were grown by a Czochralski method, are highly perfect and exhibit a large amount of extinction. Corrections for these effects are discussed. The magnetization density shows that the total moment as measured by magnetization is made up of four contributions. The moments (in μ_B) on uranium, Rh_I, Rh_{II}, and from the conduction electrons are, respectively, 0.94(3), 0.28(2), 0.03(2), and −0.11(3). The observation of a large moment at the Rh_I site, which lies in the (001) plane with the U atoms shows that strong anisotropic hybridization occurs between the U and Rh_I. This is the cause of the very large bulk anisotropy. At the uranium site we have analysed the contributions from the spin and orbital moments and find $-\mu_L/\mu_S = 1.81(7)$. The free ion $5f^3$ value for this ratio is 2.6. The reduction gives us a quantitative measure of hybridization in the system. The results are compared with those calculated from density functional theory.

1. Introduction

Extensive studies of materials containing 5f electrons (i.e. U, Np, etc) have shown that many of the physical properties are affected by a phenomenon we call 'hybridization'. What this implies is that when a uranium atom is brought together in a solid with, for example, an iron atom, it is not possible to consider the properties of the resulting solid as a simple linear combination of those of uranium and iron. Instead, a strong interaction between the outer electrons, in the case of this example between 5f and 3d electrons, occurs and can result in the compound exhibiting completely new properties. Early ideas on this hybridization are the basis for the so-called 'Hill plots' (Hill 1970). The most spectacular manifestation of these hybridization effects occurs for heavy-fermion materials, in which the ground state is superconducting at low temperature. In the case

* On leave from Departamento de Física, Universidade de Coimbra, Portugal.

0953-8984/92/030829 + 18 $03.50

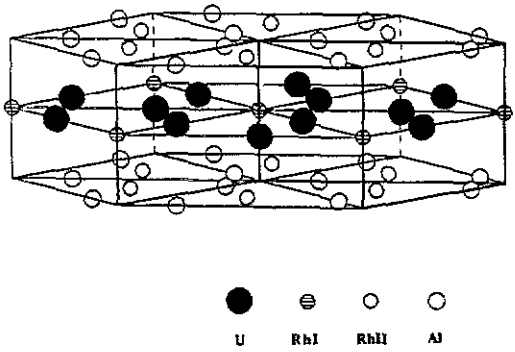

Figure 1. Schematic representation of the URhAl structure. The volume shown contains three unit cells and nine U atoms. The bold edges highlights one unit cell.

of the heavy-fermion materials it is clear that not only does hybridization occur, but also a correlated state is formed at low temperature (Stewart 1984, Ott and Fisk 1987).

In a subject as complex and general as that of 5f-electron hybridization it is clearly advantageous to be able to examine a wide range of different compounds and establish trends, which can be useful in guiding our general understanding. One of the most promising groups appears to be the AnTX group of compounds, where An is an actinide (U, Np, or Pu), T is a transition metal, and X is a p metal (Al, Ga, Sn, In, Si or Ge). Sechovsky and Havela (1988) and Sechovsky *et al* (1990) have shown that many of these form isostructural groups in which the magnetic properties vary from weak paramagnetism, spin-fluctuating systems, to stable 5f-moment systems. For example, UPdIn and UNiAl have γ-values as high as 280 and 134 mJ mol^{-1} K^{-2}, respectively, and both order antiferromagnetically with sizeable magnetic moments.

As yet there is relatively little microscopic information available about these series of compounds. Bulk properties are very important for classifying the systems; however, this information is usually insufficient to allow critical choices to be made between a number of possible theoretical approaches. We focus in this paper on the compound URhAl, and discuss in general the systems of the ZrNiAl structure, with X = Al and compounds with T = Fe, Co, Ru and Rh. URhAl becomes ferromagnetic at 27 K (Veenhuizen *et al* 1988) and has a reported γ-value of 60 mJ mol^{-1} K^{-2}. The ordered magnetic moment is $\sim 1\ \mu_B$ per formula unit, and the magnetic properties are highly anisotropic, with the easy axis being parallel to the hexagonal c-axis. Two main questions motivated our neutron measurements. (1) How is the magnetization density distributed throughout the unit cell? In particular, is there sufficient polarization of the Rh 4d wavefunctions for there to exist a moment associated with the rhodium atoms? (2) How big are the individual spin and orbital components on the uranium atom? Recently, by measuring these components in a series of intermetallic compounds with the cubic Laves phase (Lebech *et al* 1991, Lander *et al* 1991) we have shown that the ratio μ_L/μ_S can be used as a measure of the hybridization.

2. Crystallography

The ternary compound URhAl crystallizes in the hexagonal ZrNiAl structure (space group $P\bar{6}2m$), an ordered ternary derivative of the Fe_2P structure. Cell dimensions at room temperature are $a = 6.9958(34)$ Å, $c = 4.0241(62)$ Å. A schematic representation of the crystal structure is shown in figure 1. The atoms are arranged in planar layers

perpendicular to the short (c) axis, layers of Rh and Al alternating with layers of U and Rh. Atomic positions in the unit cell are as follows (Dwight *et al* 1968):

U	3g ($m2m$)	$x, 0, 1/2$	$0, x, 1/2$	$\bar{x}, \bar{x}, 1/2$	$x \approx 0.58$
Rh_I	1b ($\bar{6}2m$)	$0, 0, 1/2$			
Rh_{II}	2c ($\bar{6}$)	$1/3, 2/3, 0$	$2/3, 1/3, 0$		
Al	3f ($m2m$)	$x, 0, 0$	$0, x, 0$	$\bar{x}, x, 0$	$x \approx 0.24$

The Rh atoms occupy two distinct sites in the lattice, one third of them lying on the U–Rh layer (Rh_I site) and the remaining ones on the Al–Rh layer (Rh_{II} site). The U atoms are at the highest coordination site (CN15), the shortest distances within the coordination polyhedron being the actinide-transition metal ones ($d_{U\text{-}Rh_I} = 2.94$ Å, $d_{U\text{-}Rh_{II}} = 2.91$ Å). The in-plane U–U distance (3.63 Å) is smaller than the one in the c-direction, which is equal to the lattice parameter c. These inter-actinide distances are larger than the Hill limit (Hill 1970) and the compound orders ferromagnetically at 27 K.

Neutron experiments were performed on a cylindrical single crystal approximately 2 mm in diameter and 6 mm in length. The crystal was grown by means of a Czochralski technique and had its [001] axis approximately parallel to the cylinder axis.

A series of measurements with unpolarized neutrons were made to establish the parameters of the nuclear structure at low temperature, needed for the polarized beam work. In addition, we needed to determine the amount of extinction and verify the correct stoichiometry of our sample. The integrated intensities were measured on the D15 normal beam diffractometer at the high-flux reactor at the Institut Laue–Langevin, Grenoble. The neutrons ($\lambda = 1.176$ Å) were monochromatized with a Cu(331) crystal in transmission and the $\lambda/2$ contamination was $\approx 8 \times 10^{-4}$ of the primary beam intensity. The crystal was mounted with the [001] axis parallel to the ω-axis of the diffractometer, encapsulated in a small Al container and used in an ILL 'orange' liquid-helium cryostat. Cell parameters were refined from the UB matrix using 18 strong and well centred reflections.

Two data sets (300 K, 37 K) have been collected out to $\sin\theta/\lambda = 0.77$ Å^{-1}. The rather small c parameter of the unit cell restricted the data collection to the ($hk0$) and ($hk1$) layers. The number of independent reflections measured was 50 for the room temperature data set and 66 for the low temperature one. For each independent reflection we measured at least four and usually six, symmetry equivalent reflections. The scan profiles were analysed according to the Lehmann–Larson algorithm (Lehmann and Larson 1974) to obtain the integrated intensities. These scan profiles were found to be rather sharp, clearly indicating that our sample had a high degree of crystalline perfection. The data were corrected for the Lorentz effect and the intensities of the equivalent reflections averaged, using as weights the reciprocals of the variances derived from counting statistics. The internal agreement factors of the equivalent intensities were 1.3% and 1.1% for the room temperature and low temperature data sets, respectively. A set of nuclear structure factors was derived from the averaged intensities and their standard deviations obtained from the distribution of the equivalent intensities.

2.1. Structural refinement and extinction

Comparison between the measured structure factors and those calculated for the URhAl structure confirmed that the crystal exhibited a large amount of extinction. By extinction

we refer to the processes other than absorption that result in a reduction of intensity below the kinematical limit $I \propto |F|^2$. The average intensity loss due to this effect was about 50% reaching a maximum value of 80% for a few reflections. This is a case of strong extinction and we tried to model it according to 5 different models: the Becker–Coppens secondary extinction model with a Lorentzian or Gaussian mosaic distribution (models 1 and 2), the same model including primary extinction (models 3 and 4) (Becker and Coppens 1974a, 1974b, 1975) and the recently proposed random elastic deformation model (RED) (model 5) (Kulda 1987, 1988a). The Becker–Coppens model has as parameters the domain radius of the mosaic blocks and the width of the mosaic blocks distributions. Unlike the Becker–Coppens model that adopts the Darwin mosaic model, in RED the crystal is assumed to consist of elastically deformed domains rather than perfect blocks. This deformation is represented by a uniform bending with a constant radius R, the sign of the deformation gradient changing at random from domain to domain. The beam transport through the crystal can then be considered as a series of independent Bragg reflections on a random-walk sequence of mean free path $\bar{t}$. In its simplest form the RED extinction correction relies on these two parameters, R and $\bar{t}$, to be adjusted by fitting to a given intensity data set. A more realistic point of view considers that a deformation consists of both a misorientation and small changes of the lattice parameter. Later, the RED model has been extended to this case (Kulda 1988b). The generalization is made at the cost of one more refinable parameter, $0 \leqslant c \leqslant 1$, the limiting case $c = 0$ corresponding to a pure lattice plane misorientation.

A least-squares refinement of atomic positions, isotropic temperature factors and extinction parameters led to the results shown in tables 1 and 2. The neutron coherent scattering lengths used were $b_U = 0.8417 \times 10^{-12}$ cm, $b_{Rh} = 0.588 \times 10^{-12}$ cm and $b_{Al} = 0.349 \times 10^{-12}$ cm. The function minimized during the least-squares procedure was $\Sigma w|F_{obs} - F_{calc}|^2$, $w = 1/\sigma^2$. Anisotropic temperature factors were not refined due to the lack of (hkl) data with $l > 1$. Results of the least-squares refinements are shown in tables 1 and 2. In spite of the presence of strong extinction we were able to obtain precise values for the structural parameters. The quality of the fits are confirmed by the small R-factors obtained. The model giving the best fit to our data was the secondary extinction model of Becker–Coppens with a Lorentzian mosaic distribution (model 1) for which a final R-value of 1.8% was obtained. The inclusion of primary extinction in the Becker–Coppens formalism (models 3 and 4) did not improve the quality of the fits. Indeed, the refined values of the domain radius and mosaic spread indicate that the extinction was mostly affected by the small mosaic spread ($\eta = 1/(\sqrt{2}\,\pi g) \simeq 5 \times 10^{-3}$ min). In the low temperature data set models 3 and 4 tended to correlate the extinction parameters with unphysical negative temperature factors and have been discarded. The RED extinction model proved to work almost as well as that of Becker–Coppens giving comparable values for the structural parameters. A pure lattice plane misorientation model was used ($c = 0$) as the more general case did not improve the quality of the fit. The refined values of the parameters $\bar{t}$ and R are physically reasonable and compatible with the values for the mosaic spread found by the other models ($\eta \approx \bar{t}/R$). There was no evidence from the least-squares refinement that our sample deviated from its nominal stoichiometry.

It is well known that extinction presents as great a problem in polarized neutron studies as it does in the more conventional measurement of integrated intensities. The physical interpretation of the observations is therefore critically dependent on a proper correction for this effect. An extinction correction is judged satisfactory when the application of the extinction factors to the integrated intensities at constant temperature makes them proportional to the corresponding structure factors. The extinction plots

Table 1. Results of the least-squares refinements of URhAl data at 300 K. T and R are the parameters of the RED extinction model and r and g are the parameters of the Becker–Coppens model. $\langle y \rangle$ is the average value of the extinction correction factor ($y = I_{obs}/I_{calc}$). Lattice parameters and definitions of the least-squares figures of merit are given below the table. Models: 1—Becker–Coppens secondary extinction only, Lorentzian mosaic distribution; 2—Becker–Coppens secondary extinction only, Gaussian mosaic distribution; 3—Becker–Coppens including primary extinction, Lorentzian mosaic distribution; 4—Becker–Coppens including primary extinction, Gaussian mosaic distribution; 5—random elastic deformation model. $a = 6.9958(34)$ Å; $c = 4.0241(62)$ Å. Also

$$R\text{-factor} = \sum \frac{||F_{obs}| - |F_{calc}||}{|F_{obs}|} \qquad \chi^2 = \sum \frac{(|F_{obs}| - |F_{calc}|)^2}{N - n_{par}}.$$

Model	1	2	3	4	5
$\bar{r}$ (10^{-6} m)	—	—	—	—	246(12)
R (m)	—	—	—	—	28(3)
r (10^{-6} m)	24(4)	10(2)	16(3)	8(2)	—
g (10^4 rad^{-1})	19(4)	4.3(4)	15(5)	3.8(4)	—
U					
x/a	0.5804(2)	0.5804(3)	0.5804(2)	0.5804(3)	0.5803(2)
B (Å^2)	0.23(4)	0.33(6)	0.19(5)	0.30(6)	0.30(4)
Rh_I					
B (Å^2)	0.55(6)	0.48(9)	0.45(7)	0.46(9)	0.55(7)
Rh_{II}					
B (Å^2)	0.38(5)	0.41(7)	0.31(6)	0.40(7)	0.42(5)
Al					
x/a	0.2361(4)	0.2369(6)	0.2363(5)	0.2371(6)	0.2363(5)
B (Å^2)	0.36(5)	0.41(8)	0.30(6)	0.39(8)	0.38(6)
$\langle y \rangle$	0.50	0.61	0.55	0.62	0.59
R-factor	1.8%	2.7%	2.0%	2.8%	2.1%
χ^2	4.5	10.7	6.4	12.3	6.1

(figure 2) showing F_{obs} versus F_{calc} before and after applying the extinction correction (model 1) for the 300 K data set clearly show how successful the extinction model was in correcting for this effect. This gave us confidence that such a model could be applied to the polarized neutron data as well.

3. Onset of ferromagnetism

The intensity of the (110) reflection was monitored as a function of temperature in the range 4.7 to 37 K (figure 3). The increase of magnetic scattering below 28 K confirmed the onset of magnetic order. We estimate the transition temperature to be 28(1) K in excellent agreement with the values of 27(1) K obtained from susceptibility and specific heat data (Veenhuizen *et al* 1988). The temperature of the crystal was then lowered to 4.7 K and the same set of reflections that was measured at 37 K was remeasured at this lower temperature. The procedure to reduce the raw data to a unique set of structure factors was the same as indicated above for the other data sets. At 4.7 K the Bragg intensities, in particular those at low $\sin\theta/\lambda$, contain contributions from both nuclear

Table 2. Results of the least-squares refinements of URhAl data at 37 K. For explanation of symbols see caption of table 1. $a = 6.9808(30)$ Å; $c = 4.0063(57)$ Å.

Model	1	2	5
$\bar{t}$ (10^{-6} m)	—	—	273(13)
R (m)	—	—	18(2)
r (10^{-6} m)	37(7)	9.7(1)	—
g (10^{4} rad^{-1})	9.7(1)	3.6(4)	—
U			
x/a	0.5805(1)	0.5809(2)	0.5806(2)
B (Å^2)	0.04(5)	0.01(8)	0.01(4)
Rh_I			
B (Å^2)	0.10(7)	0.05(10)	0.04(6)
Rh_{II}			
B (Å^2)	0.06(6)	0.02(9)	0.03(6)
Al			
x/a	0.2373(4)	0.2376(6)	0.2374(6)
B (Å^2)	0.18(7)	0.16(9)	0.12(5)
$\langle y \rangle$	0.51	0.61	0.58
R-factor	2.5%	3.5%	2.3%
χ^2	12.7	26.8	13.3

and magnetic scattering. It is therefore possible to fit a magnetic model to the measured intensities, although the precision attainable is not as high as with polarized neutrons (see below). A least-squares fit of the U magnetic moment using this data set was attempted assuming a ferromagnetic alignment along the c axis. The magnetic moment was allowed to consist of a spin and orbital component. A more complete discussion of this is given in section 5. During the least-squares refinement the thermal parameters were fixed to their 37 K values and the extinction model used was the one that gave the best fit at that temperature. The U moment and its orbital component refined to $\mu = 1.08(17)\ \mu_B$ and $\mu_L = 2.1(4)\ \mu_B$, respectively, for an R factor of 2.2% ($\chi^2 = 10$). These values show that a large proportion of the U moment is of orbital origin, its spin component being coupled antiparallel to the orbital component as would be expected from Hund's rules. This value of the total moment is in excellent agreement with the results of magnetization experiments.

4. Polarized neutron experiment

4.1. Data collection

The polarized neutron measurements were made on the D3B diffractometer at ILL, Grenoble, using the same crystal that was used for the measurements of nuclear structure factors. The crystal was supported at the centre of an asymmetric split-coil superconducting magnet mounted on the diffractometer so that the c axis was approximately parallel to the ω axis of the instrument and to the applied field. The diffractometer is fitted with a detector that can be tilted out of the horizontal plane by angles up to 25° to allow reflections with scattering vectors out of the horizontal plane to be measured in

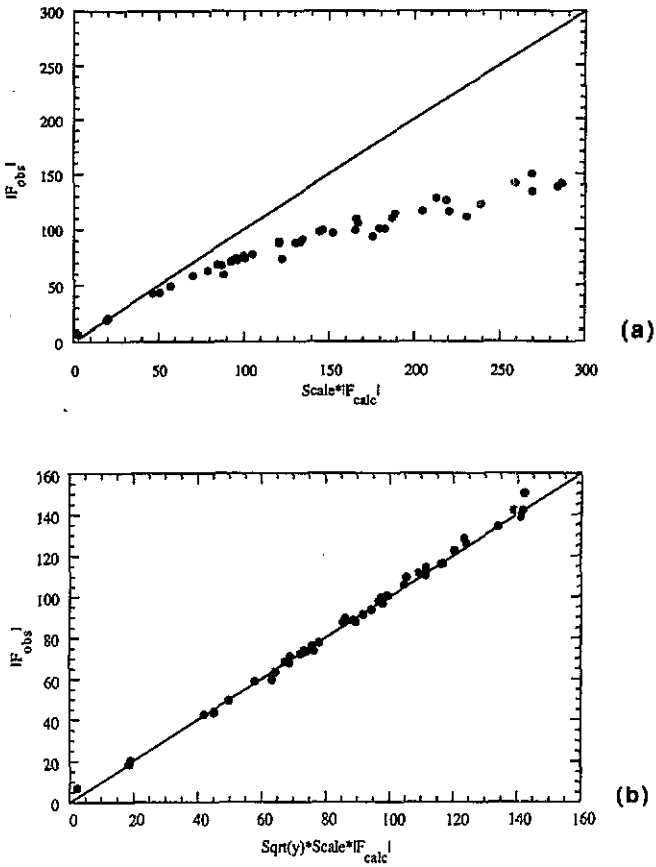

Figure 2. Plot of $|F_{obs}|$ versus scaled $|F_{calc}|$: (*a*) before applying any extinction correction; (*b*) after applying extinction correction (model 1). y is the extinction correction applying to $I_{calc} = |F_{calc}|^2$. The solid line has slope one in both figures.

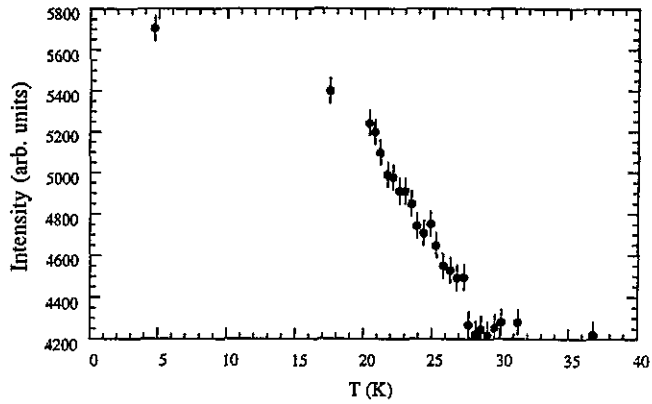

Figure 3. Intensity of the (110) reflection monitored as a function of the temperature showing the presence of magnetic scattering below 28 K.

normal beam geometry. A Heusler alloy single crystal was used to monochromatize and simultaneously polarize the neutron beam coming from the reactor hot source. We have used a wavelength of 0.843 Å for the major data collection, but wavelengths of 0.711 Å, 0.545 Å and 0.477 Å were also used in order to check the extinction correction. Suitable filters reduced the $\lambda/2$ contamination of the monochromatized beam to less than 6×10^{-3}. A Meissner–Majorana cryo-flipper with 100% efficiency was used to invert the neutron polarization. All data were taken at a stabilized temperature of 4.2 K in an applied magnetic field of 4.7 T.

4.2. Data analysis

The cross-section for elastic scattering by a ferromagnetic crystal of a beam of neutrons polarized in the direction $\hat{\boldsymbol{P}}$ is

$$\frac{\mathrm{d}\sigma}{\mathrm{d}\Omega} = N_c \frac{(2\pi)^3}{v_0} \sum_{\boldsymbol{G}} \delta(\boldsymbol{Q}-\boldsymbol{G})(N^2(\boldsymbol{Q}) + 2(\hat{\boldsymbol{P}}\cdot\boldsymbol{q})\,\mathrm{Re}(N(\boldsymbol{Q})M^*(\boldsymbol{Q})) + q^2 M(\boldsymbol{Q})^2) \tag{1}$$

where N_c is the number of cells, v_0 is the volume of the unit cell, $\boldsymbol{Q}$ is the scattering vector with $|\boldsymbol{Q}| = 4\pi \sin\theta/\lambda$, and $\boldsymbol{G}$ a reciprocal-lattice vector. N is the nuclear structure factor

$$N(\boldsymbol{Q}) = \sum_j b_j \exp(\mathrm{i}\boldsymbol{Q}\cdot\boldsymbol{r}_j)\exp(-W_j) \tag{2}$$

where the sum extends over all atoms in the unit cell with positions r_j and b and W denote the nuclear scattering length and Debye–Waller factor, respectively. The magnetic structure factor, M, is given by

$$M(\boldsymbol{Q}) = 0.2695 \sum_{j'} \mu_{j'} f_{j'}(\boldsymbol{Q}) \exp(\mathrm{i}\boldsymbol{Q}\cdot\boldsymbol{r}_{j'}) \exp(-W_{j'}) \tag{3}$$

where $\mu_{j'}$ is the magnetic moment in Bohr magnetons, $f_{j'}(\boldsymbol{Q})$ is the associated form factor and the sum is now restricted to the magnetic atoms. The numerical factor 0.2695 is the scattering length (in 10^{-12} cm units) associated with 1 μ_B. The magnetic interaction with the neutron involves the vector

$$\boldsymbol{q} = \hat{\boldsymbol{Q}} \times \hat{\boldsymbol{\mu}} \times \hat{\boldsymbol{Q}} \tag{4}$$

in which $\hat{\boldsymbol{Q}}$ and $\hat{\boldsymbol{\mu}}$ are unit vectors in the direction of the scattering vector and magnetic moment, respectively.

The polarized neutron experiment consists of measuring the Bragg intensities, first with neutrons polarized parallel to the field applied to the sample and then with reverse polarization. The ratio of these intensities gives the so-called flipping ratios, R. In the ideal case where the beam of neutrons is perfectly polarized parallel (+), then antiparallel (−) to the crystal magnetization, the ratio of the scattered intensities is

$$R = \frac{(\mathrm{d}\sigma/\mathrm{d}\Omega)^+}{(\mathrm{d}\sigma/\mathrm{d}\Omega)^-} = \frac{N^2 + 2\,\mathrm{Re}(NM^*)\sin^2\alpha + M^2\sin^2\alpha}{N^2 - 2\,\mathrm{Re}(NM^*)\sin^2\alpha + M^2\sin^2\alpha} \tag{5}$$

where α is the angle between the magnetization and the scattering vector. If the crystal structure is centrosymmetric, the structure factors are real numbers and it is possible to determine the magnetic structure factors from the measured flipping ratios, provided the nuclear structure factors are known. Solving equation (5) gives

$$\gamma = \frac{M}{N} = \frac{R+1}{R-1} \mp \sqrt{\left(\frac{R+1}{R-1}\right)^2 - \frac{1}{\sin^2\alpha}} \tag{6}$$

the selection between the two solutions being generally straightforward. However, in a non-centrosymmetric structure, as is the case of URhAl, the structure factors are in general complex quantities. In such a case the measurement of the flipping ratios alone does not determine unambiguously the magnetic structure factors, because one cannot obtain *both* real and imaginary components. We shall see how to circumvent this problem in section 4. For the moment, we consider only the subset of reflections of the form $\{h0l\}$ that do have real structure factors, because they are associated with planes where the projection of the structure is centrosymmetric. For each reflection the flipping ratio can then be converted into a magnetic structure factor, taking into account the effects of extinction, imperfect polarization and second-order contamination of the primary beam. Expression (5) for the flipping ratios becomes

$$R = \frac{[(1+p)/2]y^+(\mathrm{d}\sigma/\mathrm{d}\Omega)^+ + [(1-p)/2]y^-(\mathrm{d}\sigma/\mathrm{d}\Omega)^- + C^+_{\lambda/2}}{[(1-p)/2]y^+(\mathrm{d}\sigma/\mathrm{d}\Omega)^+ + [(1+p)/2]y^-(\mathrm{d}\sigma/\mathrm{d}\Omega)^- + C^-_{\lambda/2}} \tag{7}$$

where $0 \leqslant p < 1$ is the polarization of the beam, y^+ and y^- are the extinction corrections for the (+) and (−) cross-sections and $C^{\pm}_{\lambda/2}$ denotes the correction for the $\lambda/2$ contamination of the beam. It is a good approximation to consider this last correction independent of the neutron spin and $\simeq \frac{1}{8}(J(\lambda/2)/J(\lambda))y(\lambda/2)N^2(\lambda/2)$, where $J(\lambda)$ represents the flux of neutrons in the incident beam at wavelength λ. The polarization and second-order contamination of the beam at the four different wavelengths used have been measured using a standard technique. The extinction corrections have been made on the basis of the least-squares refinements of the 37 K data that was described in section 2. Equation (7) was solved numerically to obtain the $M(hkl)$ values for the 13 centrosymmetric reflections that were measured. For each reflection, the flipping ratios of a minimum of 4 equivalent reflections have been collected. All reflections have been measured at two different wavelengths ($\lambda = 0.843$ Å and 0.711 Å) and the strongest ones also at the shorter wavelengths of 0.545 Å and 0.477 Å. A summary of the results is given in table 3. The final observed magnetic structure factor, $M_0(hkl)$, was taken as a mean of all values and its standard deviation calculated from the distribution of the measurements. It was found that the extinction correction gave coherent results at different wavelengths, but extinction corrections remained large for the majority of reflections, even at the shortest wavelength. Correction for second-order contamination was found to be important (>10%) only for the (100) and (101) reflections. The large value of the correction for (101) (44% at $\lambda = 0.843$ Å) arises because the scattering from the (202) reflection is ≈90 times more intense than the (101).

5. Magnetization densities and U form factor

5.1. The uranium magnetic form factor

In the dipole approximation (Marshall and Lovesey, 1971), valid at low $Q = 4\pi \sin\theta/\lambda$, we can write the magnetic scattering amplitude, $\mu f(Q)$, of a uranium atom as follows:

Table 3. Summary of polarized neutron data (centrosymmetric reflections) of URhAl at $T = 4.7$ K, $H = 4.7$ T, $H \parallel c$. N is the nuclear structure factor, γ is the experimentally determined M/N ratio at $\lambda = 0.843$ Å, C_{ext} and $C_{\lambda/2}$ are respectively the extinction and second-order contamination corrections of the γ-values at this wavelength. M_o is the observed magnetic structure factor (in Bohr magnetons) and is a mean of the values measured at different wavelengths. Standard deviations in parenthesis refer to the last significant digit.

hkl	$\sin\theta/\lambda$	N	γ	C_{ext}	$C_{\lambda/2}$	M_o
100	0.0827	−0.232	0.538(9)	1.22	1.18	−0.466(5)
200	0.1654	1.392	0.350(5)	1.58	1.00	1.816(23)
300	0.2481	2.701	0.080(2)	2.04	1.00	0.770(15)
500	0.4135	2.795	0.106(4)	1.88	1.00	1.079(10)
600	0.4962	0.649	−0.166(4)	1.30	1.17	−0.396(14)
700	0.5789	2.335	0.060(2)	1.65	1.00	0.504(19)
101	0.1497	−0.149	−0.518(16)	1.40	1.44	0.246(40)
201	0.2072	−3.233	0.194(4)	2.16	1.00	−2.337(46)
501	0.4320	−2.787	0.108(1)	1.85	1.00	−1.115(8)
601	0.5117	1.152	0.082(2)	1.37	1.06	0.336(9)
701	0.5922	−3.507	0.037(2)	1.86	1.00	−0.451(32)
202	0.2994	1.390	0.299(10)	1.40	1.00	1.483(31)
302	0.3520	2.690	0.068(6)	1.82	1.00	0.703(32)

$$\mu f(Q) = \mu_S \langle j_0 \rangle + \mu_L (\langle j_0 \rangle + \langle j_2 \rangle) = \mu \langle j_0 \rangle + \mu_L \langle j_2 \rangle. \tag{8}$$

Here, μ_S and μ_L are the spin and orbital components of the magnetic moment μ. The functions $\langle j_0 \rangle$ and $\langle j_2 \rangle$ are given by

$$\langle j_n \rangle = \int_0^\infty \rho(r) j_n(Qr) 4\pi r^2 \, \mathrm{d}r \tag{9}$$

where $\rho(r)$ is the 5f electron density and j_n is the spherical Bessel function of order n. The functions $\langle j_0 \rangle$ and $\langle j_2 \rangle$ are those calculated by Desclaux and Freeman (1978) for the U^{3+} state.

5.2. *Analysis of the centrosymmetric data set*

For the centrosymmetric data set (13 reflections) the magnetic structure factors are known in magnitude and phase. As is well known, the magnetic structure factors are the Fourier components of the magnetization density in the unit cell. However a Fourier synthesis with such a limited data set will be very unreliable, due to the series termination effect of the missing Fourier components. Instead we choose to compare the observed magnetic scattering amplitudes to those calculated on the assumption that all the moment is localized on the U sites. In this approximation we have

$$M(Q) = G_U(Q) \exp(-W_U)(\mu f(Q))_U \tag{10}$$

with the geometrical structure factors

$$G_U(Q) = \sum_j \exp(\mathrm{i} Q \cdot r_j) \tag{11}$$

where the r_j denote the positions of the U atoms, W the Debye–Waller temperature

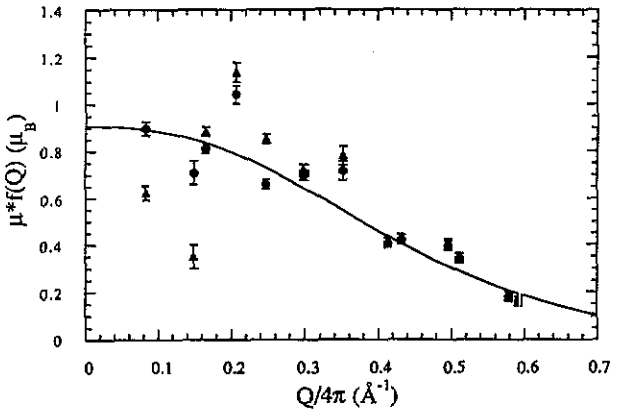

Figure 4. Centrosymmetric reflections in URhAl represented on a form factor curve as $\mu f(Q)$ versus $Q/4\pi$ ($=\sin\theta/\lambda$). The open triangles assume all the contribution comes from the U moment, whereas the solid points assume the contributions on the Rh atoms as discussed in the text. The solid line is the best fit to the latter points.

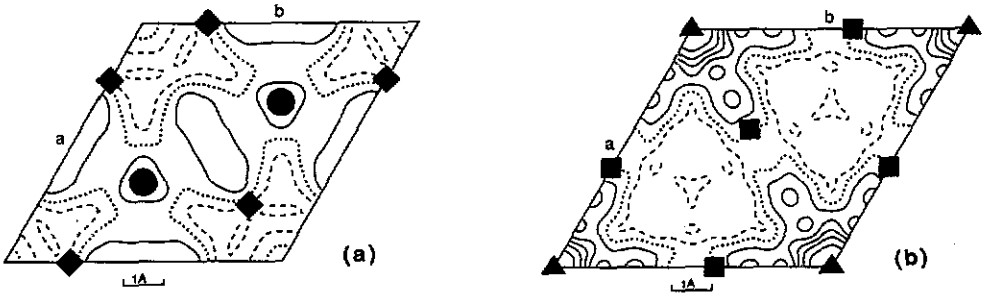

Figure 5. Difference magnetization density map obtained by Fourier synthesis, using the centrosymmetric data and the best model including only a moment at the U site. Contours at 0.010 μ_B Å^{-3}. The atom symbols are: ■, U; ▲, Rh_I; ●, Rh_{II}; ◆, Al. (*a*) Section at z = 0.0. (*b*) Section at z = 0.5.

factor and $(\mu f(Q))_U$ the uranium magnetic scattering amplitude. If $M(Q)$ is a good approximation to the observed magnetic structure factors we should expect $(\mu f(Q))_U$ to be a smooth function of Q. We used equation (10) and the observed magnetic structure factors to evaluate this function at the Bragg points. These values are shown as open triangles in figure 4. Clearly no smooth curve can be drawn through these points, especially those at low Q. The best fit of the observed structure factors to equation (10) using an isotropic U form factor, in the dipole approximation, gave $\mu = 0.90(12)\ \mu_B$, $\mu_L = 2.06(11)\ \mu_B$ and the high χ^2-value of 76. We used the U^{3+} radial functions discussed in section 5.1 above.

To obtain some insight regarding the origin of this unusual form factor, we evaluated the Fourier components $(M_o(Q) - M_c(Q))$ and performed a Fourier transform with these coefficients. This gives the difference density between the observed density and that given by the model. This density was averaged over a cube 0.5 Å edge to reduce series termination effects. Figure 5 shows the calculated difference magnetization density map

Table 4. Results of the least-squares refinement of URhAl centrosymmetric magnetic structure factors.

U:	$\mu = 0.91(9)\,\mu_B$
	$\mu_L = 2.01(8)\,\mu_B$
	$-\mu_L/\mu_S = 1.83(21)$
Rh_I:	$\mu = 0.32(9)\,\mu_B$
Rh_{II}:	$\mu = 0.09(9)\,\mu_B$

$R = 12\%$
$\chi^2 = 39$ for 13 reflections and 4 variables

in the $z = 0.0$ and $z = 0.5$ planes. The most significant feature of these maps is the presence of a positive magnetization density on the Rh_I sites. This observation suggests that a much better fit could be obtained by allowing some additional moment to be present at the Rh sites also. We therefore extended (10) to

$$M(\boldsymbol{Q}) = G_U(\boldsymbol{Q})\exp(-W_U)(\mu f(Q))_U + G_{Rh_I}(\boldsymbol{Q})\exp(-W_{Rh_I})(\mu f(Q))_{Rh_I} + G_{Rh_{II}}(\boldsymbol{Q})\exp(-W_{Rh_{II}})(\mu f(Q))_{Rh_{II}}. \quad (12)$$

The Rh form factor used was calculated from the Hartree–Fock wave function given by Clementi and Roetti (1974). Results of the least-squares fit to this expression are shown in table 4. The refinement gave a significant moment of $0.32\,\mu_B$ at the Rh_I site and a probably not significant smaller value of $0.09\,\mu_B$ at the Rh_{II} site, the χ^2 dropping to roughly half its initial value. Interestingly enough, the Rh_I sites are those located in the planes containing the U atoms. The solid points in figure 4 represent $(\mu f(Q))_U$ derived from the observed magnetic structure factors using the refined values of μ_{Rh_I} and $\mu_{Rh_{II}}$. The fit of the calculated U form factor to the experimental data is now quite acceptable, except for the reflection (201). However we should bear in mind that this reflection has the highest extinction of the complete data set ($y = 0.43$ at $\lambda = 0.477$ Å).

5.3. *Analysis of the full data set*

All reflections not belonging to the $\{h0l\}$ set have complex structure factors, and as explained in section 4.2, it is not possible to obtain the magnetic structure factors from the measured flipping ratios alone. This arises because their phases are unknown. These could be calculated if the moment was localized only at the U sites, but we have seen from the analysis of the centrosymmetric data set that this is not the case. However we can fit a magnetic model directly to the flipping ratios. The function minimized was $\Sigma\, w(R_o - R_c)^2$, $w = 1/\sigma^2$. Here R_o denotes the observed flipping ratios and R_c the values calculated using equations (3) and (9) and the magnetic structure factors given by (12). In this way both extinction and $\lambda/2$ corrections were taken into account on the calculated flipping ratios. The parameters of the model are the U moment, its orbital component, and the Rh_I and Rh_{II} moments. All measured flipping ratios were used in the refinement except reflections (201) and 111) which were rejected due to the high values of their extinction corrections. The fitting procedure converged well to a final χ^2 of 19 for 88 observations and 4 variables and a weighted R-factor on the flipping ratios of 1.9%.

Table 5. Results of the least-squares refinement on the flipping ratios data of URhAl. The full data set, except reflections (201) and (111) for reasons discussed in the text, has been used in this refinement.

U:	$\mu = 0.94(3)\ \mu_B$
	$\mu_L = 2.10(3)\ \mu_B$
	$-\mu_L/\mu_S = 1.81(7)$
Rh_I:	$\mu = 0.28(2)\ \mu_B$
Rh_{II}:	$\mu = 0.03(2)\ \mu_B$

Total moment/FU $= \mu_U + \frac{1}{3}\mu_{Rh_I} + \frac{2}{3}\mu_{Rh_{II}} = 1.05(4)\ \mu_B$.
Conduction electron polarization moment $= -0.11\ \mu_B$
$R = 3.7\%$
$\chi^2 = 19$ for 88 reflections and 4 variables

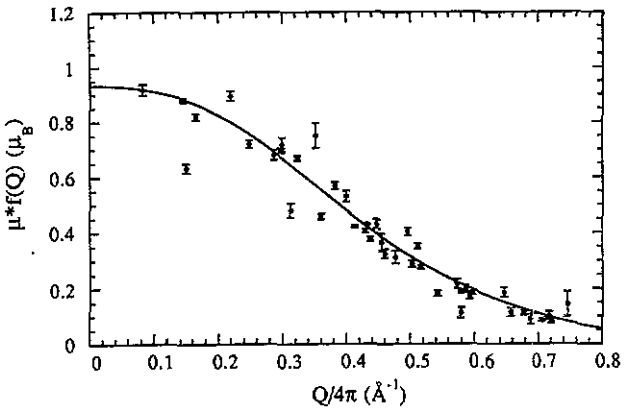

Figure 6. Form factor curve $\mu f(Q)$ for the U atom versus $Q/4\pi$ ($=\sin\theta/\lambda$). The solid points assume a contribution of 0.32 μ_B and 0.03 μ_B at the Rh_I and Rh_{II} sites, respectively. The solid line was drawn from the result of the least-squares fit.

Results of this fit are given in table 5. Refined moment values are in agreement with the results of the centrosymmetric data analysis and again a significant moment at the Rh_I site was observed. The phases of the magnetic structure factors can now be accurately computed from these results, which enables the amplitudes of the magnetic structure factors to be extracted from the measured flipping ratios. The U form factor derived from these values assuming the Rh moments as given by the least-squares fit is shown in figure 6. Difference magnetization density maps are shown in figures 7–9. The full model including the 0.28 μ_B moment at the Rh_I site and the smaller 0.03 μ_B at the Rh_{II} site reproduces the observed magnetization density quite well and the difference Fourier maps are rather featureless. On the contrary, a model with the same U contribution but without the transition metal moments shows clearly a significant positive residual at the Rh_I site and a smaller feature at the Rh_{II} site also.

6. Discussion

The main experimental difficulty in this study is concerned with the corrections for the very large extinction effects. Usually for diffraction work we can assume that the mosaic

distribution of the crystallites is relatively large, and under these conditions the scattering follows the kinematical theory with the intensity being proportional to the square of the structure factors. The other extreme is when the crystals are perfect (e.g. high quality semiconductor grade silicon) and the scattering follows the dynamical theory, with the intensity being proportional to the structure factor. Our crystals are not perfect, however, they are of sufficient quality that the kinematical theory does not describe the scattered intensity. Experimentally, these effects are minimized by choosing the shortest wavelengths for the incident radiation. For the polarized-neutron studies we have used neutrons with wavelengths as short as 0.477 Å, however, the extinction is still considerable. Following convention we have made extinction corrections. Because these are large, we believe that uncertainty in these ultimately limits the precision of the data analysis. Thus the final fits to the data have χ^2-values that are considerably higher than normally found in this type of work (e.g. a χ^2-value of 19 in table 5). The errors assigned to the observed reflections are based on counting statistics, they do not reflect the extinction effects. If we reject the strongest reflections, which always have the biggest extinction, the resulting parameters do not change appreciably, but the χ^2-values decrease.

The majority of the magnetic moment is found, as expected, on the U atom. However, a very substantial moment is found also at the Rh_I site (see table 5). Thus, the 4d electrons of Rh_I are highly polarizable, which is similar to the situation found in the intermetallic URh_3 by Delapalme *et al* (1978). This large moment at the Rh_I site is direct evidence for the hybridization between the 5f U and 4d Rh electrons. In contrast, the moment at Rh_{II} is zero within our statistical accuracy. It should be remembered here that the U–Rh_I and U–Rh_{II} distances are essentially the same (see section 2 and figure 1), so that the presence of a large moment on Rh_I, which lies in the same (001) plane as the U atom also implies that the hybridization is *anisotropic*. It is the microscopic anisotropy of the hybridization that is the origin of the bulk anisotropy. The d–f orbitals in the U–Rh_I plane hybridize strongly with their quantization axis along the *c*-axis. To turn the moments away from this axis requires that one breaks the hybridized d–f bond, and this energy far exceeds those available with applied magnetic fields. In connection with this anisotropic bonding we should expect to observe the anisotropic distribution of the magnetization density around the U atom. However, such anisotropy would give a term $\Delta C_2 \cos^2 \Theta \langle j_2 \rangle$ as the leading extra term to be added to the dipole approximation to the form factor (Lander *et al* 1984) of equation (8). Here the angle Θ is that between the scattering vector and the *c*-axis. Unfortunately the value of Θ which is 90° for reflections on the basal plane (*hk*0), does not vary sufficiently in the collected data set for us to establish the presence of a ΔC_2 term. For example, only a few reflections could be reached on the $l = 2$ layer. These arguments suggest that we should anticipate a relatively smooth form factor, see figure 6, out to sin θ/λ of about 0.6 $Å^{-1}$. The variations from such a curve in figure 6 are most probably due to the inadequacy of our extinction corrections rather than due to any real anisotropy in the magnetization density. This conclusion is further supported by the featureless difference Fourier maps we obtain after application of our model—see figures 7(*b*), 8(*b*) and 9(*b*).

The analysis of the spin and orbital components of the U atom are given in table 5. By Fourier transforming the two densities we can obtain the real space distribution of the spin and orbital moments. These, together with the total moment density, are shown in figure 10. As is well known, the spatial density of the orbital moment as observed by neutrons is more contracted in real space than the spin density. If, for uranium, the obital and spin moments are comparable in size, then the total moment density will

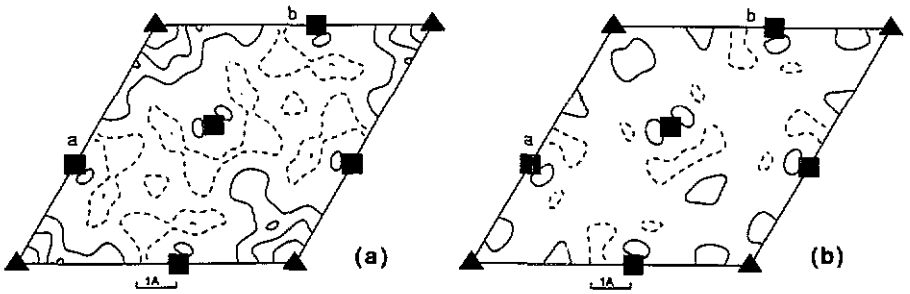

Figure 7. (*a*) Difference magnetization density map at the section $z = 0.5$ for the model without Rh contribution. Contours at 0.015 μ_B Å^{-3}. The significance level (deduced from the experimental uncertainties) is ~1 contour. The key to the atom symbols is given in figure 5. (*b*) Same section using the full model.

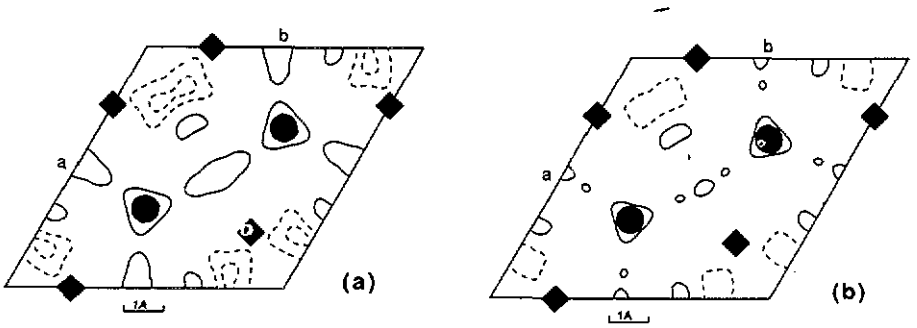

Figure 8. (*a*) Difference magnetization density map at the section $z = 0.0$ for the model without Rh contribution. Contours as in figure 7. The key to the atom symbols is given in figure 5. (*b*) Same section using the full model.

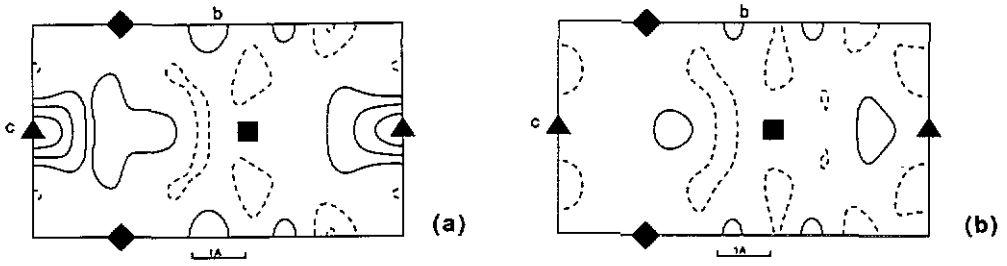

Figure 9. (*a*) Difference magnetization density map at the *yz* plane for the model without Rh contribution. Contours as in figure 7. The key to the atom symbols is given in figure 5. (*b*) Same section using the full model.

change sign as a function of distance from the nucleus. The resulting form factor has a maximum at a finite value of the momentum transfer. This is not the case here. The total integrated values we find in URhAl are $\mu_L = 2.10(3)\,\mu_B$, and $\mu_S = -1.16(3)\,\mu_B$, the value of the orbital density exceeds the absolute value of the spin density at all r. The form factor (figure 6) is 'flatter' than normal, but it does not have a 'hump'.

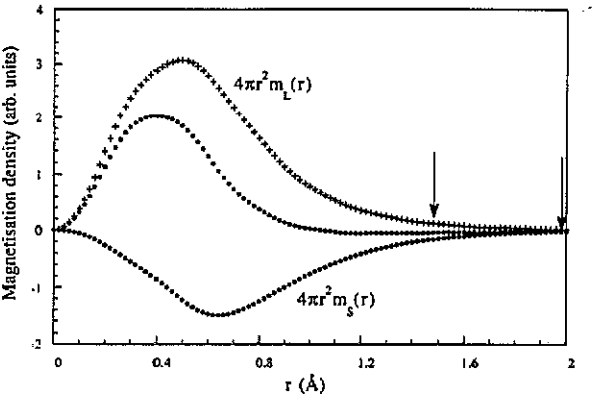

Figure 10. Schematic representation of the orbital ($4\pi r^2 m_L$) and spin ($4\pi r^2 m_S$) components of the magnetization density as a function of the distance r from the nucleus. The difference gives the total magnetization density. These curves have been obtained by Fourier transforming the μ_L- and μ_S-components of equation (1) using the $\langle j_0 \rangle$ and $\langle j_2 \rangle$ functions of Desclaux and Freeman (1978). The cut-off in the Fourier space was done at the experimental Q_{max}-value. Because of this and the inadequacy of the dipole approximation at high Q these curves are not correct in real space for small r. Thus, another node at $r < 0.3$ Å should exist. Half the nearest U–Rh and U–U distances are 1.46 and 1.98 Å, and these are marked with arrows.

The value of the ratio $-\mu_L/\mu_S$ for URhAl is 1.81(7). The free ion value for $5f^3$ is 2.6, so that the reduction from 2.6 to 1.8 is a substantial one. It is useful to plot the ratio $-\mu_L/\mu_S$ versus the f-electron count in the same manner as already performed for the actinide Laves phases by Lebech *et al* (1991). This is shown in figure 11. Following the application of density functional theory together with orbital polarization (Eriksson *et al* 1991 and references therein) we may understand the reduction of the μ_L/μ_S ratio from the free-ion value (broken line in figure 11) as a measure of the hybridization occurring between the 5f and transition-metal wavefunctions. The value for URhAl lies intermediate between that of the free ion and the cubic Laves phases. The large hybridization in the case of the Laves phases is to be expected, they are close packed with a higher coordination between the actinide and transition-metal atoms.

Gasche *et al* (1991) have performed preliminary band-structure calculations for URhAl, as well as some other materials of this structure, and included an orbital polarization term. These calculations are necessarily approximate at this stage, but they do explain, for example, why UFeAl and UCoAl are paramagnets and UNiAl is magnetic. Similarly, the rigid band model correctly predicts that URhAl should be magnetic and URuAl should not. However, beyond this point there are major differences between the calculations and the experiments. The calculated values for the total, orbital, and spin moments on the U site are (in Bohr magnetons, respectively) 0.45, 1.51, and −1.06. These are to be compared (table 5) with the experimental values of 0.94(3), 2.10(3), and −1.16(3), respectively. For the Rh_I and Rh_{II} sites the theory calculates the small moments (parallel to the U moment) of 0.04 and 0.07 μ_B per atom, respectively. In earlier work on the Laves phases (Lebech *et al* 1991, Eriksson *et al* 1991) the band-structure results were always *larger* than experiment, the results for URhAl show that this is not a general trend. The calculated ratio $-\mu_L/\mu_S$ is 1.4, again quite different from the observed value

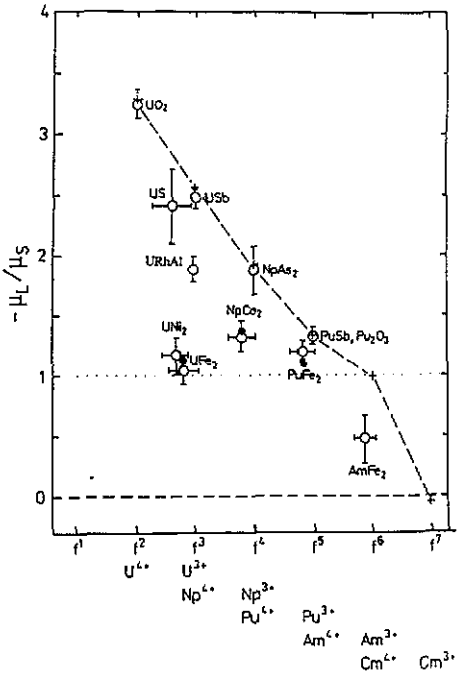

Figure 11. Dependence of the ratio between orbital μ_L and spin μ_S moments on f count in actinide materials. The crosses are derived from experimental *g*-values (Carnall and Wybourne 1964), which include intermediate coupling, and assume localized f electrons. Experimental values derived from neutron experiments are shown as open circles. The values derived from band structure calculations are shown as solid circles.

of 1.8. However, we should not expect this to be in agreement at this early stage. The experiments have pointed to one important shortcoming of the theory in its present form, and this is related to the anisotropic bonding, which gives rise to the much larger moment at the Rh_I site than at the Rh_{II} site. At present, the theory uses spherical potentials and averaging procedures, which proved adequate for the high symmetry of the cubic Laves phase structure, but which are certainly a poor approximation in the present layered-like structure.

The compound UCoAl is isostructural with URhAl and isoelectronic in the sense that Rh is below Co in the periodic table. UCoAl, in contrast to URhAl, does not order magnetically, but is a strongly enhanced paramagnet. For a field of 5 T Wulff *et al* (1990) were able to induce a moment of $\sim 0.35\,\mu_B$ per mole, and they measured the magnetization density in the unit cell. As with our study, they found the principal magnetization on the U atom with a small effect (~15%) on the Co atoms. In their preliminary report Wulff *et al* (1990) report the centrosymmetric reflections only (11 of them) and with such a limited data set did not attempt to refine separately the Co_I and Co_{II} site moments. Delapalme (1991) has recently refined the complete data set and shown that the largest effects are on the Co_I site. This feature is in good agreement with our study of URhAl. The experimental value of μ_L/μ_S (from the reduced data set) is 2.7(5), which is not significantly different from the free ion value (2.6). The theoretical value is 1.7. Although the full experimental analysis is not yet available for UCoAl, it would appear that the hybridization is smaller than in URhAl. This is expected as the 4d Rh wavefunctions are more expanded than the 3d wavefunctions of Co, leading to a higher degree of hybridization for the 4d series. In this respect we are now

undertaking an experimental study of URuAl, which should show even greater hybridization effects.

Acknowledgments

We thank Mike Brooks and Tom Gasche for interesting discussions on the theoretical aspects of the hybridization. One of us (JAP) would like to acknowledge the ILL, Grenoble, for the provision of facilities used for this work.

References

Becker P J and Coppens P 1974a *Acta Crystallogr.* A **30** 129
—— 1974b *Acta Crystallogr.* A **30** 148
—— 1975 *Acta Crystallogr.* A **31** 417
Carnall W T and Wybourne B G 1964 *J. Chem. Phys.* **40** 3428
Clementi E and Roetti C 1974 *At. Data Nucl. Data Tables* **14** 178
Delapalme A 1991 private communication
Delapalme A, Lander G H and Brown P J 1978 *J. Phys. C: Solid State Phys.* **11** 1441
Desclaux J P and Freeman A J 1978 *J. Magn. Magn. Mater.* **8** 119
Dwight A E, Mueller M H, Conner Jr R A, Downey J W and Knott H 1968 *Trans. Metall. Soc. AIME* **242** 2076
Eriksson O, Brooks M S S, Johansson B, Albers R C and Boring A M 1991 *J. Appl. Phys.* **69** 5897
Gasche T, Auluck S, Brooks M S S and Johansson B 1991 *Proc. Int. Conf. on Magnetism (Edinburgh, UK, 1991)*; *J. Magn. Magn. Mater.* at press
Hill H H 1970 *Plutonium and other Actinides* vol 2, ed W N Moner (New York: AIMA) p 2
Kulda J 1987 *Acta Crystallogr.* A **43** 167
—— 1988a *Acta Crystallogr.* A **43** 283
—— 1988b *Acta Crystallogr.* A **44** 286
Lander G H, Brooks M S S and Johansson B 1991 *Phys. Rev.* B **43** 13672
Lander G H, Delapalme A, Brown P J, Spirlet J C, Rebizant J and Vogt O 1984 *Phys. Rev. Lett.* **53** 2262
Lebech B, Wulff M and Lander G H 1991 *J. Appl. Phys.* **69** 5891
Lehmann M S and Larson F K 1974 *Acta Crystallogr.* A **30** 580
Marshall W and Lovesey S W 1971 *Theory of Thermal Neutron Scattering* (Oxford: Oxford University Press) p 152
Ott H R and Fisk Z 1987 *Handbook on the Physics and Chemistry of the Actinides* vol 5, ed A J Freeman and G H Lander (Amsterdam: North-Holland) p 85
Sechovsky V and Havela L 1988 *Ferromagnetic Materials* ed E P Wohlfarth and K H J Buschow (Amsterdam: North-Holland) p 309
Sechovsky V, Havela L, Nozar P, Brück E, de Boer F R, Menovsky A A, Buschow K H J and Andreev A V 1990 *Physica* B **163** 103
Stewart G R 1984 *Rev. Mod. Phys.* **56** 755
Veenhuizen P A, Klaasse J C P, de Boer F R, Sechovsky V and Havela L 1988 *J. Appl. Phys.* **63** 3064
Wulff M, Fournier J M, Delapalme A, Gillon B, Sechovsky V, Havela L and Andreev A V 1990 *Physica* B **163** 331